Impact of the kinetic boundary condition on porous media flow in the lattice Boltzmann formulation

Shiwani Singh,[1,*] Fei Jiang,[1,2] and Takeshi Tsuji[1,3]

[1]*International Institute for Carbon-Neutral Energy Research (WPI-I^{2}CNER), Kyushu University, Fukuoka, Japan*

[2]*Department of Mechanical Engineering, Graduate School of Sciences and Technology for Innovation, Yamaguchi University, Japan*

[3]*Department of Earth Resources Engineering, Kyushu University, Fukuoka, Japan*

(Received 31 October 2016; published 7 July 2017)

To emphasize the importance of the kinetic boundary condition for micro- to nanoscale flow, we present an *ad hoc* kinetic boundary condition suitable for torturous geological porous media. We found that the kinetic boundary condition is one of the essential features which should be supplemented to the standard lattice Boltzmann scheme in order to obtain accurate continuum observables. The claim is validated using a channel flow setup by showing the agreement of mass flux with analytical value. Further, using a homogeneous porous structure, the importance of the kinetic boundary condition is shown by comparing the permeability correction factor with the analytical value. Finally, the proposed alternate to the kinetic boundary condition is validated by showing its capability to capture the basic feature of the kinetic boundary condition.

DOI: 10.1103/PhysRevE.96.013303

I. INTRODUCTION

An understanding of the transportation processes and fluid flow through geological porous media helps in various engineering applications, for instance, gas transport, oil extraction, CO_2 sequestration, and many more [1,2]. The transport of fluid depends largely on the geometry and structure of the pores. Depending on the pore size, the fluid behavior can be divided into four major regimes: continuum flow regime with $\mathrm{Kn} < 0.001$ (Knudsen number Kn is the ratio of the molecular mean free path with respect to character macroscopic length), slip flow regime with $0.001 < \mathrm{Kn} < 0.1$, transition flow regime with $0.1 < \mathrm{Kn} < 10$, and free molecular flow regime with $\mathrm{Kn} > 10$.

The typical length scales of pores in the conventional oil field is of the order of a few micrometers. Furthermore, the advent of unconventional energy resources such as tight gas, shale gas, etc. has attracted focus towards the fluid flow on an even smaller scale (of the order of nanometers) [3,4]. The flow behavior in these narrow pores is completely different from the continuum flow. At finite Kn, many of the continuum approximations break down, hence, the plain Navier-Stokes solvers with no-slip boundary conditions may not be valid. For example, as the pore size decreases, permeability, which is a key factor in the evaluation of the transport capacity of porous media, becomes higher than that expected from Darcy's law. This phenomenon was first proposed by Kinkenberg [5], who suggested that the increase is due to the increase of gas slippage occurring at the solid-fluid interface. Therefore, any numerical scheme should incorporate the properties such as slip at the solid-fluid interface in order to accurately predict flow behavior in narrow pores.

In the last two decades, the lattice Boltzmann method (LBM) has emerged as an effective tool to simulate the hydrodynamics of Newtonian fluids following the Navier-Stokes equation [6–9]. The LBM can be understood as an approximate technique for solving the discrete Boltzmann equation based on the single relaxation Bhatnagar-Gross-Krook (BGK) approximation [10]. Using the multiscale Chapman-Enskog asymptotic expansion, it can be shown that the lattice Boltzmann equation reproduces the Navier-Stokes equation in the vanishing Kn limit [11]. Therefore, at small Kn limit, the validity of LBM is guaranteed. However, for finite Kn flow, where the molecular mean free path becomes comparable to pore size, the applicability of the scheme is only partially understood. The finite Knudsen flow is governed by Burnett and super-Burnett equations, which are the higher order generalized hydrodynamic equations. The numerical applicability of these equations is limited due to practical difficulties [12,13].

Through various attempts over the past few years, it is now recognized that in order to recover the basic features of noncontinuum flow, the appropriate kinetic boundary condition is need for gas kinetic schemes [14,15]. Also, the kinetic origin of LBM motivated Ansumali and Karlin [16] to introduce a diffusively reflecting solid wall boundary condition, which can be understood as a direct discretization of the classical diffuse scattering boundary condition for the Boltzmann equation. Unlike the bounce-back boundary condition where the incident particle is directly reversed, the main concept behind the kinetic boundary condition is that the particle which strikes a solid wall is reflected back randomly following Maxwellian distribution. Prior attempts have been made to incorporate a second-order accurate slip effect using a mixture of bounce-back and kinetic boundary conditions with a heuristic tuning parameter [17–19]. However, properly choosing this parameter is still an open question and the boundary condition is restricted to straight geometry. Later, Tao and Guo [20] proposed a mixed boundary condition for the curved boundaries in which the heuristic parameter is selected by tuning the constant of the multiple relaxation time (MRT) lattice Boltzmann scheme to achieve proper slip. Although the kinetic boundary condition is helpful in reducing numerical instability, due to the need to calculate the wall normal $\boldsymbol{n}$ towards the fluid, the application of this boundary condition is restricted to the flat geometry [16,21,22].

In this paper, we focus on the importance of the kinetic boundary over curved surfaces using a simplified homogeneous porous media. We show that the kinetic boundary

*shiwani@i2cner.kyushu-u.ac.jp

condition is one of the essential ingredients in the lattice Boltzmann scheme to obtain both bulk and local features of a fluid flow at finite Kn. Due to the large burden of calculating surface normal, this boundary condition is not suited for torturous porous geometry usually encountered in geological rocks. Therefore, as a next step, we introduced an *ad hoc* kinetic boundary condition which does not require the information of the normal direction. This *ad hoc* kinetic boundary condition is constructed by tagging the wall boundary with outgoing flux and is shown to retain the basic features of the kinetic boundary condition, at least in the slip and early-transition regime.

The paper is organized as follows: The LBM is briefly reviewed in Sec. II. The diffuse reflection kinetic boundary condition as proposed by Ansumali and Karlin [16] is reviewed and, using the channel flow setup, its importance for the flow at finite Kn number is highlighted in Sec. III. This simulation scheme is extended for the simple porous media between two parallel plates in Sec. IV, followed by the introduction of the *ad hoc* boundary condition, which is based on the mechanism used initially to construct the kinetic boundary condition. In Sec. V, it is shown that for the porous media flow also, the kinetic boundary is necessary to obtain the correct value of permeability and the correct local velocity profile, at least until the early-transition flow. Finally, the work is summarized in Sec. VI.

II. LATTICE BOLTZMANN METHOD

In a typical LBM framework, one works with a set of discrete populations $f = \{f_i\}$, corresponding to predefined discrete velocities $\boldsymbol{c}_i$ $(i = 1, \ldots, N)$ [6,23]. The discrete form of the governing equation is

$$f_i(\boldsymbol{x} + \boldsymbol{c}\Delta t, t + \Delta t) = f_i(\boldsymbol{x}, t) + \Omega_i(f) + \Delta t F_i, \quad (1)$$

where $\Omega_i(f)$ is the discrete collision operator generally expressed by a single relaxation time approximation or the lattice BGK approximation (LBGK),

$$\Omega_i(f) = \frac{\Delta t}{\tau}\left[f_i^{\mathrm{eq}} - f_i(\boldsymbol{x}, t)\right], \quad (2)$$

which corresponds to the relaxation of the distribution function to an equilibrium Maxwell-Boltzmann function, f^{eq}, as given in Eq. (3), at the rate of τ^{-1},

$$f_i^{\mathrm{eq}} = w_i \rho\left[1 + \frac{\boldsymbol{c}_i \cdot \boldsymbol{u}}{c_s^2} + \frac{(\boldsymbol{c}_i \cdot \boldsymbol{u})^2}{2\, c_s^4} - \frac{(\boldsymbol{u} \cdot \boldsymbol{u})}{2\, c_s^2}\right]. \quad (3)$$

In Eq. (3), w_i is the weight associated with the discrete equilibrium distribution function, c_s is the lattice sound speed, ρ is the local density, and $\boldsymbol{u}$ is the local velocity. The term F_i in Eq. (1) is the contribution of the body force and is given as [24]

$$F_i = w_i \rho\left[\frac{\boldsymbol{g} \cdot \boldsymbol{c}_i}{c_s^2} + \frac{(\boldsymbol{g}\boldsymbol{u} + \boldsymbol{u}\boldsymbol{g}) : (\boldsymbol{c}_i\boldsymbol{c}_i - c_s^2\boldsymbol{\delta})}{2c_s^2}\right], \quad (4)$$

where $\boldsymbol{g}$ is the constant acceleration vector. For implementation purposes, Eq. (1) can be divided into two basic operations as follows.

(i) Collision:

$$f_i^{\star}(\mathbf{x}, t) = f_i(\mathbf{x}, t) + \frac{\Delta t}{\tau}\left[f_i^{\mathrm{eq}} - f_i(\boldsymbol{x}, t)\right] + \Delta t F_i. \quad (5)$$

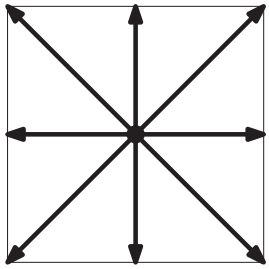

FIG. 1. D2Q9 discrete-velocity model.

(ii) Free streaming:

$$f_i(\mathbf{x}, t + \Delta t) = f_i^{\star}(\boldsymbol{x} - \mathbf{c}\Delta t, t). \quad (6)$$

The desired local macroscopic observables such as density (ρ), momentum density ($\rho\boldsymbol{u}$), and momentum flux ($\boldsymbol{\Pi}$) can be obtained from the discrete distribution function as

$$\begin{aligned} \rho(\boldsymbol{x}, t) &= \sum_i f_i, \\ \rho(\boldsymbol{x}, t)\boldsymbol{u}(\boldsymbol{x}, t) &= \sum_i f_i \boldsymbol{c}_i, \\ \boldsymbol{\Pi}(\boldsymbol{x}, t) &= \sum_i f_i \left(\boldsymbol{c}_i\boldsymbol{c}_i - c_s^2\boldsymbol{\delta}\right), \end{aligned} \quad (7)$$

where $\boldsymbol{\delta}$ is the identity matrix. In the limit of vanishing Kn number, the multiscale Chapman-Enskog (CE) expansion yields the Navier-Stokes equations to the second order. The CE expansion also reveals the relation between the relaxation time (τ) and the kinematic viscosity (η) of the fluid as $\eta = c_s^2(\tau - \Delta t/2)$. The D2Q9 velocity model (D stands for spatial dimension and Q stands for discrete velocity), as shown in Fig. 1, is used in the present study. It has the following discrete velocities $\boldsymbol{c}_i$:

$$\boldsymbol{c}_i = \begin{cases} (0,0) & \text{if } i = 0 \\ \left[\cos\frac{(i-1)\pi}{4}, \sin\frac{(i-1)\pi}{4}\right] & \text{if } i = 1,2,3,4 \\ \sqrt{2}\left[\cos\frac{(i-1)\pi}{4}, \sin\frac{(i-1)\pi}{4}\right] & \text{if } i = 5,6,7,8, \end{cases} \quad (8)$$

with the corresponding weights as

$$w_i = \begin{cases} \frac{4}{9} & \text{for } i = 0 \\ \frac{1}{9} & \text{for } i = 1,2,3,4 \\ \frac{1}{36} & \text{for } i = 5,6,7,8. \end{cases} \quad (9)$$

In order to make this scheme more robust and stable, a regularization procedure was introduction in the BGK framework (RLBGK) by Chen and co-workers [25,26] and Latt and Chopard [27] which basically removes the information of undesired higher order moments. A brief summary of this procedure is given in Appendix A.

III. KINETIC BOUNDARY CONDITION

One of the major issues when dealing with fluid flow at finite Kn is choosing the appropriate boundary condition. In the conventional bounce-back boundary condition, the directions of the incoming distribution functions are reversed when it encounters the boundary node. This boundary condition mimics the no-slip condition in the continuum limit (low Kn).

However, as the Kn increases, slippage effects starts to appear at the boundaries and the no-slip assumption is not accurate. Hence, with increasing Kn, the failure of the bounce-back boundary condition is inevitable.

Recognizing this shortcoming of LBGK for small-scale flow and exploiting the kinetic origin of LBM, a diffusively reflecting solid wall boundary condition was proposed by Ansumali and Karlin [16]. The basic idea behind this boundary condition is to redistribute the populations coming towards the wall such that it follows mass-balance and normal-flux conditions. The discrete version of the boundary condition is

$$f_i(\boldsymbol{x}_w,t) = K f_i^{\mathrm{eq}}(\rho,\boldsymbol{u}_w), \tag{10}$$

where subscript w denotes the wall and

$$K = \frac{\sum_{\boldsymbol{c}_i\cdot\boldsymbol{n}<0} |(\boldsymbol{c}_i - \boldsymbol{u}_w)\cdot\boldsymbol{n}| f_i}{\sum_{\boldsymbol{c}_i\cdot\boldsymbol{n}>0} |(\boldsymbol{c}_i - \boldsymbol{u}_w)\cdot\boldsymbol{n}| f_i^{\mathrm{eq}}(\rho,\boldsymbol{u}_w)}, \tag{11}$$

with $\boldsymbol{n}$ being the unit normal direction. The term K can be understood as the ratio of total outgoing flux to the wall and total incoming equilibrium flux from the wall. This interpretation of the term K will be utilized later in Sec. IV to construct a suitable boundary condition for porous media. Furthermore, Tao and Guo [20] recently proposed a diffuse bounce-back boundary condition (DBB) where second-order accurate slip flow is analytically established in straight flow by using a combination of the bounce-back boundary condition and the kinetic boundary. A brief introduction of DBB is given in Appendix B.

Flow between parallel plates

In order to see the effect of the kinetic boundary condition, we first consider the two-dimensional, viscous flow between two stationary parallel plates (plane Poiseuille flow) that are separated by a distance h. The Kn for this flow is $\eta/(h\,c_s)$, where the kinematic viscosity is defined as $\eta = c_s^2(\tau - \Delta t/2)$. The simulation is performed using 20 grid points to discretize the channel height h. By keeping the mean velocity U_0 small, we attain a nominal Mach number, $\mathrm{Ma} = U_0/c_s$, of the order of 10^{-6} to enforce incompressibility. This in turn results in small Reynolds number, $\mathrm{Re} = \mathrm{Ma}/\mathrm{Kn}$, which is in compliance with the Darcy limit. In Fig. 2, the normalized mass flux, $Q = \sum_0^h u_x(y)/Q_0$ with $Q_0 = gh^2/c_s$, is plotted with increasing Kn for the kinetic boundary condition (KB), bounce-back boundary condition (BB), and diffuse bounce-back scheme (DBB). The labels used in Fig. 2 to describe the simulation based on the BGK model with and without regularization are RLBGK and LBGK, respectively. The label MRT is used to denote the simulation with a multirelaxation time scheme with $\tau_q = 1$, where τ_q is associated with the relaxation of heat flux in the multirelaxation model (for more details, see Appendix B). The mass flux results are also compared with the direct simulation Monte Carlo (DSMC) results taken from Ref. [28].

As can be seen from Fig. 2, for continuum flow ($\mathrm{Kn} \to 0$), mass flux evaluated from every scheme is almost the same. However, as Kn starts to increase, the bounce-back boundary condition without regularization (BB-LGBK) initially underestimates the mass flux until around $\mathrm{Kn} \approx 0.3$ and then overestimates it in the transition flow regime. On the other hand, the bounce-back boundary condition in the BGK scheme with regularization (BB-RLGBK) as well as the bounce-back boundary condition in the MRT scheme (BB-MRT) almost give the same value of mass flow as predicted by Navier-Stokes with the no-slip boundary condition which is $Q = 1/(12\,\mathrm{Kn})$.

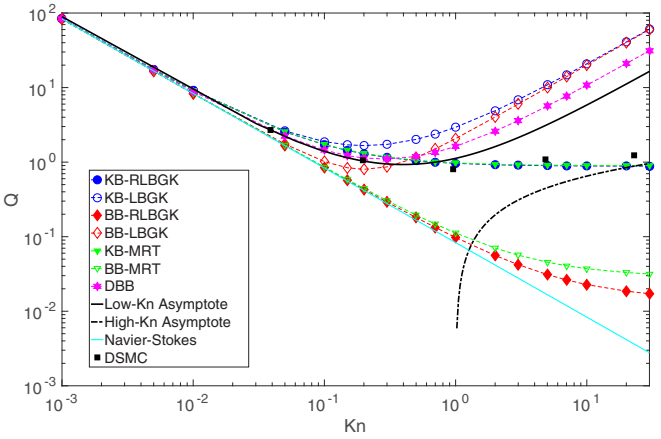

FIG. 2. Normalized mass flux (Q) as a function of Kn, using different models. KB stands for kinetic boundary condition, BB stands for bounce-back boundary condition, and AKB stands for *ad hoc* kinetic boundary condition. RLBGK stands for regularized LBGK and MRT stands for the multirelaxation scheme with $\tau_q = 1$. DBB stands for the diffuse bounce-back boundary condition of the multirelaxation time scheme.

Further, the kinetic boundary condition in the BGK scheme without regularization (KB-LGBK) always overestimates the value. The kinetic boundary condition with regularization (KB-RLGBK) as well as the kinetic boundary condition in the MRT scheme (KB-MRT) match well with the DSMC results and analytical solution given by Cercignani [11] in the low Kn limit,

$$Q_{\mathrm{low}} = \frac{1}{2}\left[\frac{1}{6\mathrm{Kn}} + s + (2s^2 - 1)\mathrm{Kn}\right], \quad \text{with } s = 1.01615, \tag{12}$$

as well as high Kn limit,

$$Q_{\mathrm{high}} = \frac{\ln(\mathrm{Kn})}{2\sqrt{\pi}}. \tag{13}$$

It is worth noting at this point that results obtained by RLGK and those obtained by the MRT scheme are similar. This is not surprising because the regularization process in which the undesired nonhydrodynamic modes are suppressed can also be considered as a multirelaxation process in which the hydrodynamic moments are relaxed at a rate which is associated with viscosity and, at the same time, the nonhydrodynamic modes are eliminated by relaxing them with a unit rate (in this case, $\tau_q = 1$) [29,30]. Finally, the diffused bounce-back boundary condition (DBB) which is designed to capture the flow accurately in the slip regime matches perfectly with the low Kn asymptote; however, it starts to deviate after $\mathrm{Kn} = 0.2$. Hence, it can be concluded that the kinetic boundary condition plays a major role in both BGK and MRT schemes of the lattice Boltzmann method in order to obtain the correct nonequilibrium behavior [28,31].

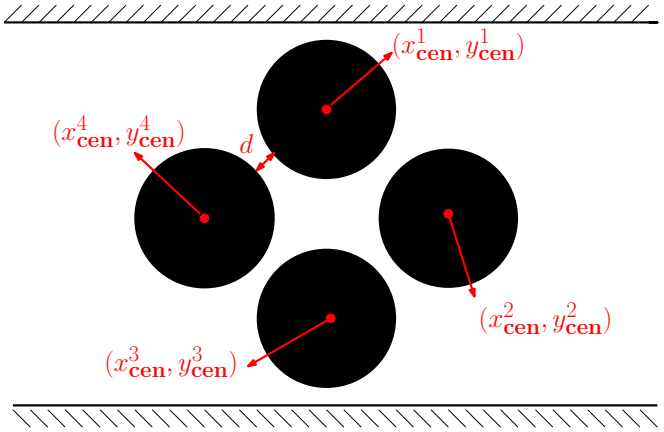

FIG. 3. Porous media model with pore-throat diameter d.

IV. KINETIC BOUNDARY CONDITION FOR POROUS MEDIA

The encouraging result discussed in the previous section inspired us to investigate the finite Knudsen effects in porous media flow using the LB framework. To test the applicability of the kinetic boundary condition, we consider a simple connected porous media model between the parallel plate, as shown in Fig. 3. In order to define the Kn, the characteristic length is taken to be the pore-throat diameter d, as shown in the figure. The centers of the four circles used to construct the porous media are also identified and labeled as $(x^i_{\text{cen}}, y^i_{\text{cen}})$ with $i = 1$

In order to apply the kinetic diffuse reflection boundary condition, first recall Eq. (10) which says that the distribution function moving towards the fluid from a stationary wall node ($\boldsymbol{u}_w = 0$) should be updated as

$$f_i(\boldsymbol{x}_w, t) = K f_i^{\text{eq}}, \tag{14}$$

where

$$K = \frac{\sum_{A_i<0} |A_i| f_i}{\sum_{A_i>0} |A_i| f_i^{\text{eq}}}, \tag{15}$$

with $A_i = c_{ix} n_x + c_{iy} n_y$. This boundary condition requires the knowledge of normal direction $\boldsymbol{n}$ towards the fluid for implementation, which has restricted its use for plane geometry. The objective now is to find the normal direction at the boundary node. For this purpose, the whole domain is divided into solid phases labeled i (corresponding to the ith circle) and the fluid phase which is set to be 0. The node $\boldsymbol{x}$ is identified as fluid-boundary node $\boldsymbol{x}^i_b$ of the ith circle if $\boldsymbol{x} = 0$ and $\boldsymbol{x}_N = i$, where N stands for the neighboring node on the grid. Then, the unit normal for a perfect circle is calculated as

$$\hat{\boldsymbol{n}}^i = \frac{\boldsymbol{x}^i_b - \boldsymbol{x}^i_{\text{cen}}}{\left|\boldsymbol{x}^i_b - \boldsymbol{x}^i_{\text{cen}}\right|}. \tag{16}$$

Ad hoc kinetic boundary condition

The calculation of the unit normal for a regular geometry such as the one shown in Fig. 3 is straightforward. However, the porous media encountered in natural rock have very complex geometry. Therefore, it is desirable to introduce a boundary condition which does not require the information of the normal direction. The boundary condition as given by Eq. (14) can still be used, but the term K which is the ratio of total outgoing flux to the wall and total incoming equilibrium flux from the wall (as mentioned in Sec. III) can be assumed as

$$K = \frac{\text{Flux}_{\text{out}}}{\text{Flux}^{\text{eq}}_{\text{in}}}. \tag{17}$$

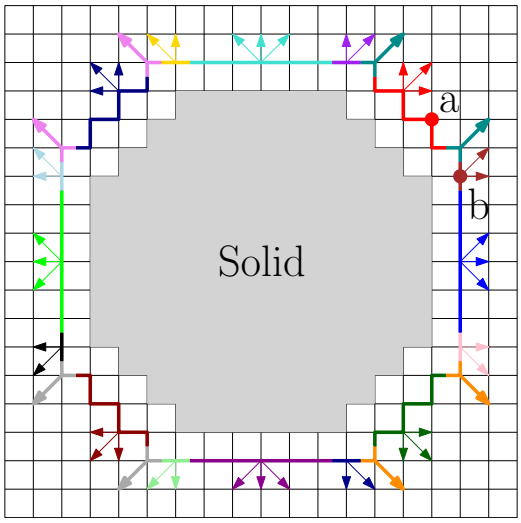

FIG. 4. Each color identifies the boundary node depending on the outgoing velocity distribution. The arrows represents the directions of the distribution function to be corrected at a particular boundary node.

To implement this boundary, we first need to label the boundary node based on the specific distribution functions moving towards fluid away from the wall. A pictorial representation of the same on a coarser grid is given in Fig. 4. Different color on the boundary node signifies the different outgoing flux. To further illustrate the implementation, two points (a and b) on the boundary node are chosen.

At the boundary node a, the term K is given as

$$K_a = \frac{f_{\swarrow} + f_{\leftarrow} + f_{\downarrow}}{f^{\text{eq}}_{\nearrow} + f^{\text{eq}}_{\rightarrow} + f^{\text{eq}}_{\uparrow}}, \tag{18}$$

and the boundary condition implementation is given as

$$f_{\nearrow} = K_a f^{\text{eq}}_{\nearrow}, \quad f_{\rightarrow} = K_a f^{\text{eq}}_{\rightarrow}, \quad f_{\uparrow} = K_a f^{\text{eq}}_{\uparrow}. \tag{19}$$

Similarly, at boundary node b,

$$K_b = \frac{f_{\swarrow} + f_{\leftarrow}}{f^{\text{eq}}_{\nearrow} + f^{\text{eq}}_{\rightarrow}}, \tag{20}$$

and

$$f_{\nearrow} = K_b f^{\text{eq}}_{\nearrow}, \quad f_{\rightarrow} = K_b f^{\text{eq}}_{\rightarrow}. \tag{21}$$

This boundary condition will be tested in Sec. V to check its capability to be used in place of the actual kinetic boundary condition for a real porous media. Moreover, the real pore geometry of natural rocks is usually obtained from micro-CT images, which generate only pixel or voxel data and not the explicit boundary curve between the pore and solid [32,33]. The proposed *ad hoc* kinetic boundary condition is very

suitable for this kind of data and can be directly applied to binarized CT images. In this boundary condition, rather than calculating the approximated boundary curve and then the normal direction, a preprocess operation can be performed to store a direction list for the boundary nodes, which makes it computationally more efficient.

V. FLOW BETWEEN PARALLEL PLATE FILLED WITH POROUS MEDIA

To comply with incompressibility and the Darcy limit, the Reynold and Mach numbers are kept low. For the case of creeping flow (Re $\rightarrow$ 0), permeability (κ), the physical quantity of interest in porous media flow, is defined using Darcy's law as

$$\kappa = \frac{Q\mu}{\rho g}, \tag{22}$$

where Q is the mass flux per unit length across the channel, μ is the dynamic viscosity, g is the body force, and ρ is the density of the fluid. With an objective to test the ability of the kinetic boundary condition to capture the microscale and nanoscale flows, the permeability with different Kn number is calculated. The permeability correction factor (PCF) which is defined as the ratio of apparent permeability (κ) with absolute permeability (κ_0) is plotted in Fig. 5. To calculate the absolute permeability for each scheme in the limit of Kn $\rightarrow$ 0, we extrapolated the permeability calculated within the range from Kn $= 10^{-1}$ to Kn $= 10^{-3}$ and chose the value at 10^{-7} as κ_0. In the present study, we have considered a regular geometry; however, in geological sites, one encounters heterogeneous and torturous rock structure. In that scenario, this strategy of calculating absolute permeability could also be useful because of the absence of any analytical formula for arbitrary structure.

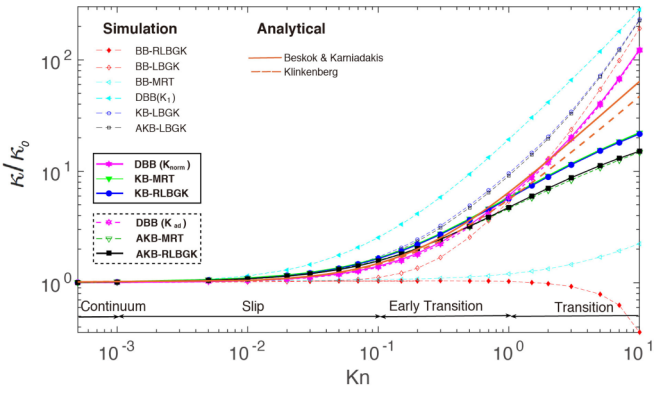

FIG. 5. Permeability correction factor with increasing Kn number. DBB (K_1) denotes the diffuse bounce-back implementation where K is set to one as proposed in Ref. [20], DBB (K_{norm}) denotes the DBB scheme where K is calculated using information of the normal direction [Eq. (15)], and DBB (K_{ad}) denotes the DBB scheme where K is calculated using the proposed *ad hoc* scheme [Eq. (17)]. The rest of the labels have the same meaning as defined in Fig. 2. The methods marked within the solid rectangle are the ones with the kinetic boundary condition which are in best agreement with the analytical results, and those within the dashed rectangle are with the *ad hoc* kinetic boundary condition.

The simulations were performed with 500 grid points in each direction. Recall that the Kn number in this case is defined as Kn $= \eta/(dc_s)$. Hence, the Kn is changed by tuning η. The analytic correction factors proposed by Klinkenberg [5],

$$\frac{\kappa}{\kappa_0} = 1 + 4c\text{Kn}, \tag{23}$$

and Beskok *et al.* [34],

$$\frac{\kappa}{\kappa_0} = [1 + \alpha(\text{Kn})\text{Kn}]\left(1 + \frac{4\text{Kn}}{1 + \text{Kn}}\right), \tag{24}$$

are taken as a reference. Here, c is set to be 1 and the rarefaction coefficient α(Kn) is given as

$$\alpha(\text{Kn}) = \frac{1.358}{1 + 0.170\,\text{Kn}^{-0.4348}}. \tag{25}$$

In order to describe the results obtained in Fig. 5, the Kn range is divided into four flow regimes as below:

(i) Continuum flow regime (Kn < 0.001): For the low Kn (continuum) limit, each scheme yields almost the same value of permeability correction factor.

(ii) Slip flow regime ($0.001 <$ Kn < 0.1): The bounce-back boundary condition in all the schemes (LBGK, RLBGK, and MRT) does not predict any increase in the value of permeability from absolute permeability. The kinetic boundary condition and *ad hoc* kinetic boundary condition (KB-LBGK, KB-RLBGK, AKB-LBGK, AKB-RLBGK, KB-MRT, and AKB-MRT) slightly overpredict PCF after Kn $= 0.01$, however still remaining in the agreement with the analytic results. On the other hand, simplified diffuse bounce-back boundary condition DBB(K_1) overestimates the permeability in the slip regime itself. The diffuse bounce-back boundary condition and its *ad hoc* version, DBB(K_{norm}) and DBB(K_{ad}), perfectly fit the analytical solution.

(iii) Early-transition flow regime ($0.1 <$ Kn < 1.0): In this regime, the bounce-back boundary condition in the BGK scheme with regularization (BB-RLBGK) as well as the bounce-back boundary condition in the multirelaxation scheme (BB-MRT) do not predict a significant increase in the permeability. The BGK implementation without regularization (BB-LBGK) shows the increase in apparent permeability; however, it largely underpredicts the PCF as compared to the analytical value. The kinetic boundary condition as well as the *ad hoc* kinetic boundary condition in the MRT scheme and BGK with the regularization scheme (KB-MRT, AKB-MRT, KB-RLBGK, and AKB-RLBGK) provide the permeability correction factors which are reasonably comparable to the analytical value. On the other hand, the kinetic boundary condition and the *ad hoc* kinetic boundary condition without regularization in the BGK formulation (KB-LBGK and AKB-LBGK) significantly overestimate the value of PCF. It should be noted that the *ad hoc* kinetic boundary condition underpredicts the PCF values as compared to those obtained using the kinetic boundary condition. The simplified diffuse bounce-back boundary condition DBB(K_1) continues to overestimate the permeability in this regime also. The diffuse bounce-back boundary condition and its *ad hoc* version, DBB(K_{norm}) and DBB(K_{ad}), lie between between the Beskok and the Klinkenberg solutions.

(iv) Transition flow regime ($1 < \mathrm{Kn} < 10$): Finally, in the transition regime, the bounce-back boundary condition with regularization in the BGK framework (BB-RLBGK) predicts a lower value of absolute permeability as compared to the apparent permeability after $\mathrm{Kn} = 5.0$, which definitely is an unphysical prediction. The bounce-back boundary condition in the multirelaxation scheme (BB-MRT) predicts permeability slightly above one. All of the other simulations except with the kinetic and *ad hoc* kinetic boundary conditions with regularization in the BGK and MRT schemes overestimate the value of the permeability correction. These schemes (KB-RLBGK, AKB-RLBGK, KB-MRT, and KB-AKB) start to significantly underestimate the analytical value after $\mathrm{Kn} = 2.0$.

Again it can be seen from Fig. 5 that the regularized BGK and MRT ($\tau_q = 1$) produce similar results as expected. The above-mentioned discussion indicates that the kinetic boundary condition is one of the essentials for modeling flow in slip and early-transition regimes under the LB framework. For the flow beyond this limit, one needs to consider the higher order lattice, as suggested by Montessori *et al.* [28]. This aspect of the scheme is left for future study.

After investigating the bulk properties (permeability), it is natural to see how the local observables behave under different boundary conditions. Therefore, the steady state streamlines are plotted first for the diffuse bounce-back boundary condition in Fig. 6 and then for the three boundary conditions (BB, KB, AKB) in the BGK scheme, without regularization in Fig. 7 and with regularization in Fig. 8, for different Kn. The same scale has been used for all the plots to show the difference in the prediction of the velocity field made by different boundary conditions. For small Kn ($\mathrm{Kn} = 0.05$), the streamlines obtained from all three boundary condition are similar.

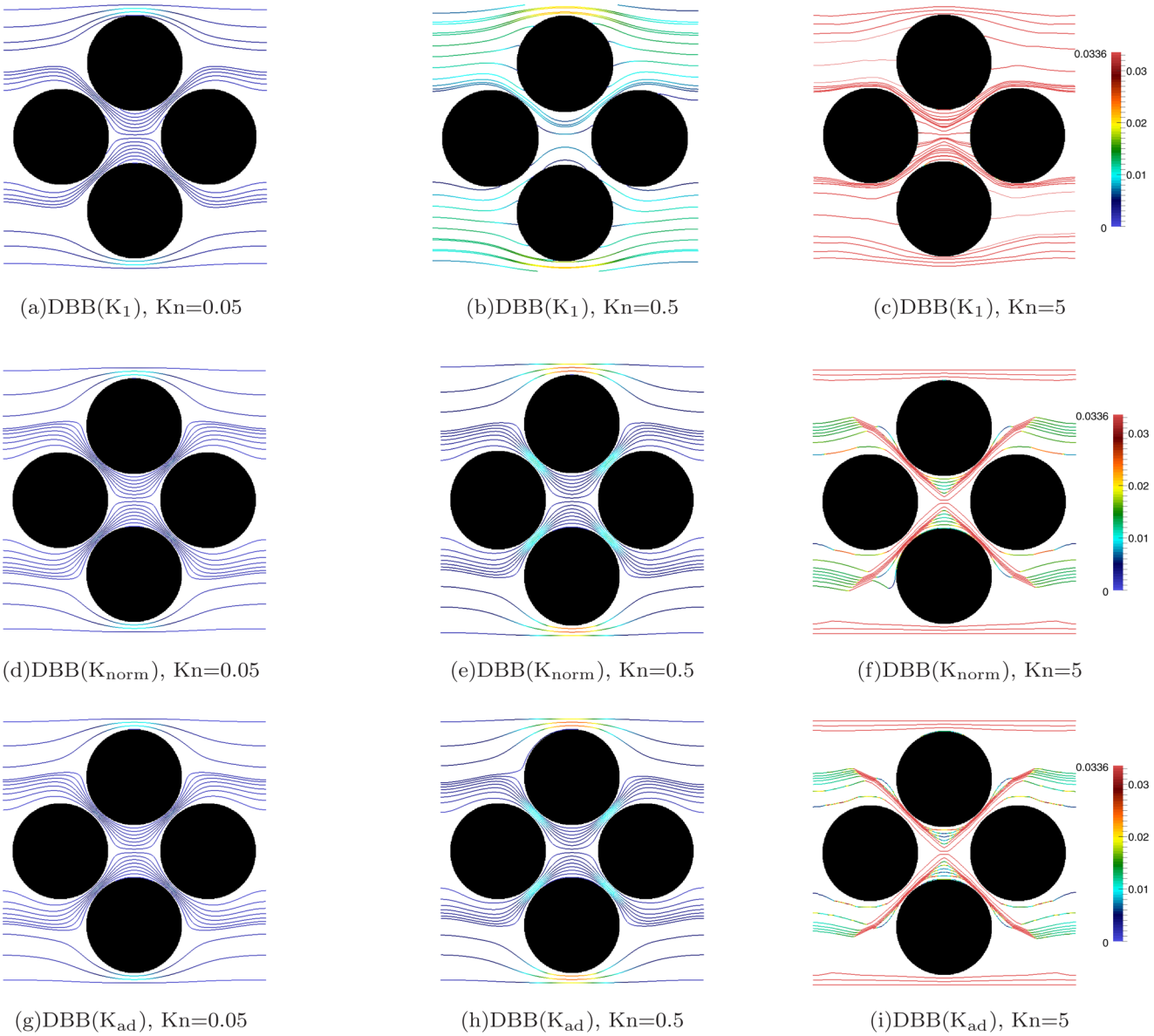

FIG. 6. Steady state velocity streamlines with diffuse bounce-back boundary condition (DBB) with K obtained in three ways: K_1 [Figs. 6(a)–6(c)], K_{norm} [Figs 6(d)–6(f)], and K_{ad} [Figs. 6(g)–6(i)], for different Kn numbers.

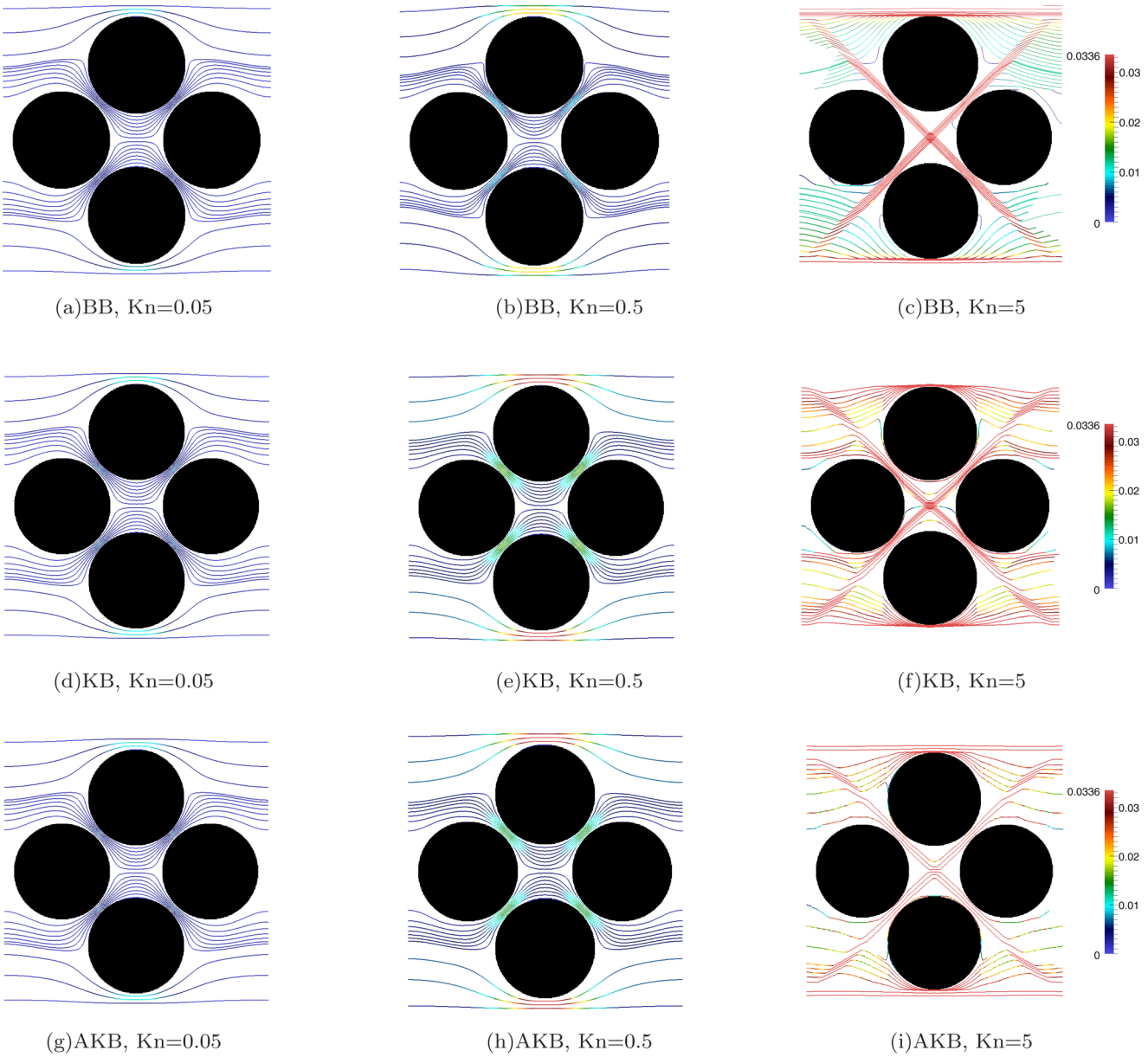

FIG. 7. Steady state velocity streamlines in the BGK scheme without regularization for different boundary conditions and Kn numbers.

(i) DBB scheme: The simplified diffuse bounce-back boundary condition DBB(K_1) does not predict accurate results even in the early transition regime [see Figs. 6(b) and 6(c)]. The boundary implementation in which information of the normal direction is needed as well as its *ad hoc* version, which works well in the early transition regime, but fails after it.

(ii) BGK (LBGK) scheme: As the Kn number is increased (Kn $= 0.5$), the bounce-back boundary condition does not show any increase of velocity between the pores, as can be seen from Fig. 7(b). The kinetic boundary condition as well as *ad hoc* boundary condition shows an increase in velocity between the pores [see Figs. 7(e) and 7(h)]. However, as the Kn number is further increased to 5, all three boundary conditions fail to produce any reasonable flow profile.

(iii) Regularized BGK (RLBGK) scheme: The kinetic boundary condition and *ad hoc* kinetic boundary condition efficiently capture the flow profile even at high Kn number, as shown in Figs. 8(f) and 8(i). The bounce-back boundary condition at Kn $= 5.0$ produces unphysical vortices at the boundaries. This proves that the bounce-back boundary condition completely fails at high Kn number.

As can be seen from Figs. 8(d)– 8(f), with the increase in Kn, the magnitude of velocity increases inside the pore throat. This increase of velocity can be attributed to the increase of slip velocity with increasing Kn around the boundaries, whose effect will be maximum inside the pore throat.

At this point, we can conclude that although by design the diffused bounce-back boundary condition (DBB) is second-order accurate in the slip regime, its simplified version DBB(K_1), where the ratio of the outgoing to incoming equilibrium flux, K, is set to one, does not reproduce accurate bulk as well as local properties. The true diffused bounce-back boundary condition DBB(K_{norm}), where K is calculated based on the information of local normals and its *ad hoc* version

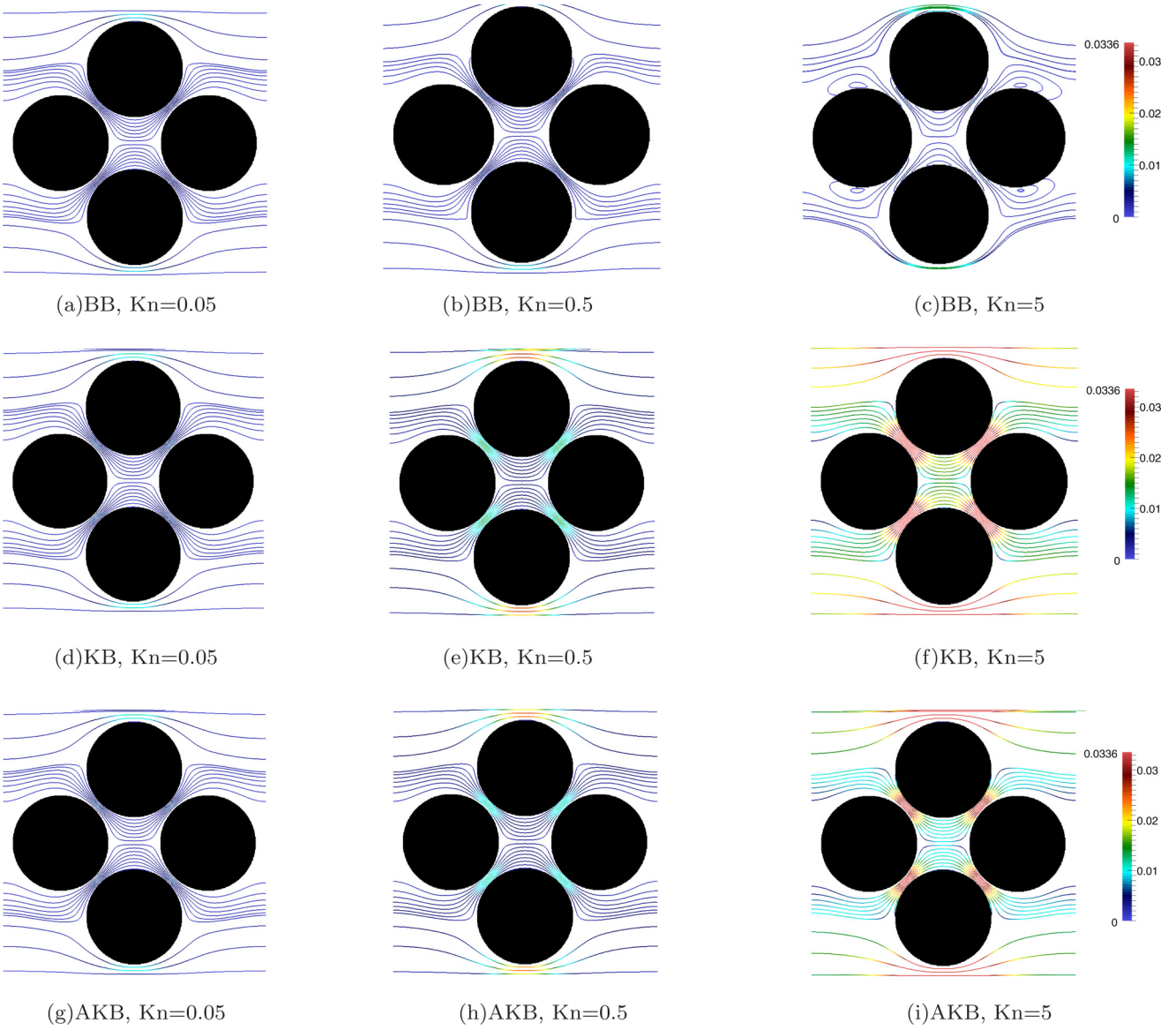

FIG. 8. Steady state velocity streamlines in the BGK scheme with regularization for different boundary conditions and Kn numbers.

DBB (K_{ad}), gives accurate predictions in the slip regime. At the same time, the kinetic and *ad hoc* kinetic boundary conditions with regularization in the BGK scheme work well, at least for the slip and early-transition regimes, both in terms of bulk and local variable. Also, in the transition regime, when other numerical schemes fail to produce the correct local flow profile, the kinetic and *ad hoc* kinetic boundary conditions with regularization in the BGK framework reproduce a reasonably accurate flow profile. It should be noted that the velocity in the pore throat, in Fig. 8, is slightly less for the *ad hoc* kinetic boundary condition as compared to the kinetic boundary condition (KB). Therefore, it is instructive to investigate the slip velocity generated by different boundary conditions. For this purpose, a point is chosen between the pores, as shown in Fig. 9. From now on, we only consider the case with the regularization scheme in the BGK framework. At this marked location, the steady state velocity is calculated as

$$u_{\text{pore}} = \sqrt{u_x^2 + u_y^2}. \tag{26}$$

The u_{pore} is plotted with increasing Kn in Fig. 9(b). As expected, the bounce-back boundary condition does not predict any significant increase of slip velocity with increasing Kn. Although both the kinetic and *ad hoc* boundary conditions

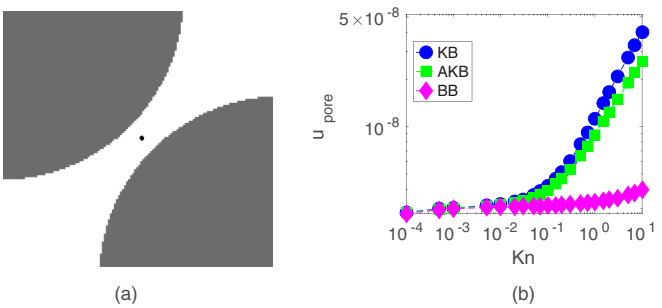

FIG. 9. (a) A point of observation is marked inside the pore to study the (b) magnitude of local velocity with the KB and AKB conditions.

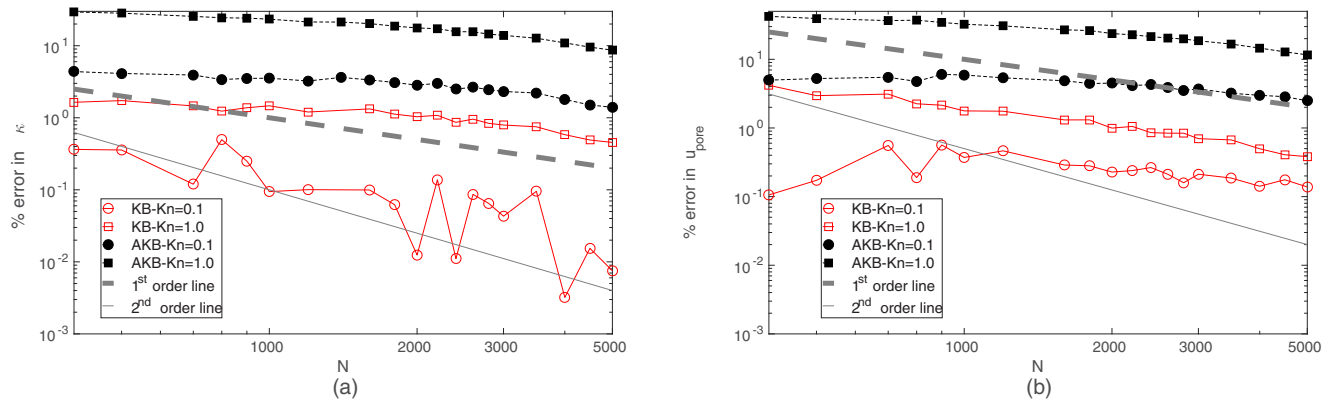

FIG. 10. Grid convergence study for the KB and AKB conditions. (a) The percentage error in κ and (b) the percentage error in u_{pore}. To provide an estimate of the accuracy, the first- and the second-order accurate lines are also plotted.

show an expected increase in velocity in the pore with increasing Kn, the *ad hoc* kinetic boundary condition starts to severely deviate from and underpredicts the value obtained from the KB after the slip flow regime. Hence, to estimate the effect of discretization error present in the *ad hoc* boundary, it is helpful to do the grid convergence study on both the bulk and local observables. The percentage error in permeability (κ) and and pore-throat velocity (u_{pore}) with different grid resolution (N) are calculated as

$$\%\ \text{error in}\ \kappa = \left|\frac{\kappa^N - \kappa^\infty}{\kappa^\infty}\right| \times 100 \quad \text{and}$$

$$\%\ \text{error in}\ u_{\text{pore}} = \left|\frac{u^N_{\text{pore}} - u^\infty_{\text{pore}}}{u^\infty_{\text{pore}}}\right| \times 100, \tag{27}$$

where the converged values κ^∞ and u^∞_{pore} correspond to the limit $dX \to 0\,(N \to \infty)$, with dX being the grid spacing.

The percentage error in the permeability and velocity inside the pore throat are plotted in Figs. 10(a) and 10(b), respectively, at two Kn: Kn = 0.1 and Kn = 1.0. As can be seen from the figures, for low Kn (Kn = 0.1), the percentage error in both κ and u_{pore} obtained using the kinetic boundary condition, although fluctuating, is too small (below 0.5) to significantly affect the continuum observables. For Kn = 1, the kinetic boundary condition yields the percentage error in κ which is only slightly above 1 for small number of grid points. The percentage error in u_{pore} for this value of Kn starts with around 5% for small resolution, but converges quickly to 1 as the grid point is increased. The *ad hoc* kinetic boundary condition (AKB) at Kn = 0.1 yields around 5% error in both κ and u_{pore} for small resolution, which decreases with increasing grid size. However, for Kn = 1.0, the percentage error in both κ and u_{pore} is more than 10 for an even reasonably large number of grid points. This suggests that the *ad hoc* kinetic boundary condition (AKB) predicts the flow reasonably well with small resolution until the slip flow regime, but for the early-transition regime, a large number of grid points is needed to get correct flow properties.

VI. CONCLUSION AND OUTLOOK

In this paper, we explore the feasibility of using the lattice Boltzmann for micro- to nanoscale porous flows. The significance of the kinetic boundary is first highlighted by showing its ability to produce correct mass flux in both low and high Kn limit in the channel flow setup in the existing slip model, both in BGK and MRT schemes of the lattice Boltzmann method. Further, the implementation of the kinetic boundary is presented in a simple homogeneous porous geometry by calculating the wall normal around curved boundaries. It is shown to capture the inherent physics of the slip and early-transition limit, such as Kn-dependent permeability and correct local velocity profile. Furthermore, realizing the difficulties of its usage in a realistic geological porous structure, an alternate boundary condition is proposed. This boundary condition is constructed by tagging the wall with outgoing flux instead of evaluating wall normal and is shown to reproduce the basic flow characteristics as shown by the kinetic boundary condition. To sum up, the correct implementation of the kinetic boundary condition, either by calculation of the surface normal or in an *ad hoc* manner as proposed here, or in a somewhat equivalent manner [35], is crucial in micro- to nanoscale flows.

The average pore size in the conventional geological sites is of the order of a few micrometers [33] and, with a mean free length of gases such as CO_2 and CH_4 in tens of nanometers [36], the gas flow in geological porous media falls under the slip regime. Therefore, in order to predict the accurate storage capacity of a geological site, we cannot ignore the slip effect. In such scenario, it is important to use the kinetic boundary condition if one chooses to use the lattice Boltzmann method to make numerical predictions of flow. The porous geometry in two dimensions is considered in the present work; however, the extension of the boundary condition to three dimensions is straightforward. In subsequent work, we will study the slip effect of the fluid flow in a realistic porous geometry of natural rock imaged by a multislice micro-CT scanner [32].

ACKNOWLEDGMENTS

The authors are grateful for the support of the International Institute of Carbon-Neutral Energy Research (WPI-I2CNER), sponsored by the Japanese Ministry of Education, Culture, Sports, Science and Technology. This study was supported by JSPS through a Grant-in-Aid for Scientific Research on Inno-

vative Areas (Grants No. 15H01143 and No. 17H05318) and a Grant-in-Aid for Young Scientists (Grant No. 16K18331).

APPENDIX A: REGULARIZATION PROCEDURE

One of the major shortcomings of the LBGK is the loss of stability with decreasing viscosity (high Re) for applications of practical importance. In order to address this shortcoming, a modification in the existing LBGK was introduced by Chen and co-workers [25,26] and Latt and Chopard [27], called the regularized BGK method. The motivation behind regularization was to filter out the higher order nonhydrodynamics or ghost modes, which will remove the unphysical effect responsible for inducing instability in the macroscopic flow. To do so, the poststreaming distribution function is divided into two parts,

$$f_i = f_i^{\mathrm{eq}} + f_i^{\mathrm{neq}}. \tag{A1}$$

Here, f_i^{eq} contains only the information of hydrodynamic moments. However, in order to eliminate the contribution of nonhydrodynamics mode, f_i^{neq} is converted to a new distribution function f^{Reg} which is defined only in the terms of hydrodynamically relevant moments (ρ,$\boldsymbol{u}$,$\boldsymbol{\Pi}$). The discrete form of f^{Reg} turns out to be

$$f_i^{\mathrm{Reg}} = \frac{w_i}{2c_s^4}\left(\boldsymbol{c}_i\boldsymbol{c}_i - c_s^2\boldsymbol{\delta}\right) : \boldsymbol{\Pi}^{\mathrm{neq}}, \tag{A2}$$

where $\boldsymbol{\Pi}^{\mathrm{neq}}$ is the nonequilibrium part of momentum flux and is defined as $\boldsymbol{\Pi}^{\mathrm{neq}} = \sum_i f^{\mathrm{neq}}(\boldsymbol{c}_i\boldsymbol{c}_i - c_s^2\boldsymbol{\delta})$. The regularized version of the BGK-based lattice Boltzmann method takes the following form:

$$f_i(\boldsymbol{x} + \boldsymbol{c}\Delta t, t + \Delta t) = f_i^{\mathrm{eq}} + \left(1 - \frac{\Delta t}{\tau}\right) f_i^{\mathrm{Reg}} + \Delta t F_i. \tag{A3}$$

Using RLGBK, not only an improvement in the convergence rate for a given Re but also a higher stable Re simulation for a given grid resolution are achieved [29]. In other words, an important gain in quality and numerical stability is obtained at very low cost. Although regularization was first introduced to devise a more stable BGK scheme, later on it was recognized as one of the key factors essential in finite Kn flows [28,37,38].

APPENDIX B: DIFFUSED BOUNCE-BACK BOUNDARY CONDITION

In the multiple relaxation time scheme of the lattice Boltzmann method, the collision term used in Eq. (1) is given as

$$\Omega_i^{\mathrm{MRT}} = \sum_j (\boldsymbol{M}^{-1}\boldsymbol{S}\boldsymbol{M})_{ij}\left(f_j - f_j^{\mathrm{eq}}\right), \tag{B1}$$

where the transformation matrix $\boldsymbol{M}$ is given by [39]

$$\boldsymbol{M} = \begin{bmatrix} 1 & 1 & 1 & 1 & 1 & 1 & 1 & 1 & 1 \\ -4 & -1 & -1 & -1 & -1 & 2 & 2 & 2 & 2 \\ 4 & -2 & -2 & -2 & -2 & 1 & 1 & 1 & 1 \\ 0 & 1 & 0 & -1 & 0 & 1 & -1 & -1 & 1 \\ 0 & -2 & 0 & 2 & 0 & 1 & -1 & -1 & 1 \\ 0 & 0 & 1 & 0 & -1 & 1 & 1 & -1 & -1 \\ 0 & 0 & -2 & 0 & 2 & 1 & 1 & -1 & -1 \\ 0 & 1 & -1 & 1 & -1 & 0 & 0 & 0 & 0 \\ 0 & 0 & 0 & 0 & 0 & 1 & -1 & 1 & -1 \end{bmatrix}, \tag{B2}$$

with the diagonal relaxation matrix $\boldsymbol{S}$ being given as

$$\boldsymbol{S} = \mathrm{diag}\{\tau_\rho, \tau_e, \tau_\epsilon, \tau_d, \tau_q, \tau_d, \tau_q, \tau_s, \tau_s\}^{-1}, \tag{B3}$$

where τ_ρ and τ_d can take any value and τ_s determines the shear viscosity and τ_e determines the bulk viscosity. The value of τ_e is taken as 1.1 and τ_ϵ as 1.2, in accordance with Ref. [20]. Since the values of τ_e and τ_ϵ have negligible influence on the simulation results, one can choose to work with a similar but efficient two relaxation time (TRT) scheme [40,41]. The value of τ_q is taken as one in the present study. However, in a recently proposed diffused bounce-back condition [20], a combination of the bounce-back (BB) and kinetic boundary (KB) conditions is used as

$$f_{\mathrm{boundary}} = r f_{\mathrm{BB}} + (1 - r) f_{\mathrm{KB}}, \tag{B4}$$

in which the combinational coefficient r and the relaxation parameter associated with heat flux, τ_q, are tuned using the first- and second-order slip coefficients of the channel flow to achieve the second-order accurate slip model. The explicit expressions used in Refs. [20,42] (for the specific case of $\Delta = 1/2$) for r and τ_q are

$$\begin{aligned} r &= \frac{\sqrt{6/\pi} - C_1}{\sqrt{6/\pi} + C_1}, \\ \tau_q &= \frac{C_2\pi}{4}(\tau_s - 0.5) + \frac{3}{16(\tau_s - 0.5)} + 0.5, \end{aligned} \tag{B5}$$

where the first-order and second-order slip coefficients are taken as $C_1 = [(1 - 0.1817\sigma)(2 - \sigma)]/(\sigma)$ and $C_2 = 1/\pi + C_1^2/2$, respectively [20]. Here the wall accommodation factor σ is chosen as one.

[1] O. D. Bert Metz, H. de Coninck, M. Loos, and L. Meyer, IPCC Special Report on Carbon Dioxide Capture and Storage, (Cambridge University Press, Cambridge, 2005).

[2] K. Michael, A. Golab, V. Shulakova, J. Ennis-King, G. Allinson, S. Sharma, and T. Aiken, Geological storage of CO_2 in saline aquifers: A review of the experience from existing storage operations, Int. J. Greenhouse Gas Control **4**, 659 (2010).

[3] F. Javadpour, D. Fisher, and M. Unsworth, Nanoscale gas flow in shale gas sediments, J. Can. Pet. Technol. **46**(10) (2007).

[4] C. M. Freeman, G. J. Moridis, and T. A. Blasingame, A numerical study of microscale flow behavior in tight gas and shale gas reservoir systems, Transp. Porous Media **90**, 253 (2011).

[5] L. Klinkenberg, in *Drilling and Production Practice* (American Petroleum Institute, Washington, D.C., 1941).

[6] R. Benzi, S. Succi, and M. Vergassola, The lattice Boltzmann equation theory and applications, Phys. Rep. **222**, 145 (1992).

[7] S. Chen and G. D. Doolen, Lattice Boltzmann method for fluid flows, Annu. Rev. Fluid Mech. **30**, 329 (1998).

[8] S. Succi, *The Lattice Boltzmann Method for Fluid Dynamics and Beyond* (Oxford University Press, Oxford, 2001).

[9] C. K. Aidun and J. R. Clausen, Lattice-Boltzmann method for complex flows, Annu. Rev. Fluid Mech. **42**, 439 (2010).

[10] P. L. Bhatnagar, E. P. Gross, and M. Krook, A model for collision processes in gases. I. Small amplitude processes in charged and neutral one-component systems, Phys. Rev. **94**, 511 (1954).

[11] Carlo Cercignani, *Theory and Application of the Boltzmann Equation* (Scottish Academic Press, Edinburgh and London, 1975).

[12] R. K. Standish, Numerical evidence for divergent Burnett coefficients, Phys. Rev. E **60**, 5175 (1999).

[13] R. K. Agarwal, K. Y. Yun, and R. Balakrishnan, Beyond Navier-Stokes: Burnett equations for flows in the continuum–transition regime, Phys. Fluids **13**, 3061 (2001).

[14] Taishan Zhu and Wenjing Ye, Theoretical and numerical studies of noncontinuum gas-phase heat conduction in micro/nano devices, Numer. Heat Transfer, Part B **57**, 203 (2010).

[15] Hongwei Liu, Kun Xu, Taishan Zhu, and Wenjing Ye, Multiple temperature kinetic model and its applications to micro-scale gas flows, Comput. Fluids **67**, 115 (2012).

[16] S. Ansumali and I. V. Karlin, Kinetic boundary conditions in the lattice Boltzmann method, Phys. Rev. E **66**, 026311 (2002).

[17] S. Succi, Mesoscopic Modeling of Slip Motion at Fluid-Solid Interfaces with Heterogeneous Catalysis, Phys. Rev. Lett. **89**, 064502 (2002).

[18] Z. Guo, B. Shi, T. S. Zhao, and C. Zheng, Discrete effects on boundary conditions for the lattice Boltzmann equation in simulating microscale gas flows, Phys. Rev. E **76**, 056704 (2007).

[19] Frederik Verhaeghe, Li-Shi Luo, and Bart Blanpain, Lattice Boltzmann modeling of microchannel flow in slip flow regime, J. Comput. Phys. **228**, 147 (2009).

[20] S. Tao and Z. Guo, Boundary condition for lattice Boltzmann modeling of microscale gas flows with curved walls in the slip regime, Phys. Rev. E **91**, 043305 (2015).

[21] W. P. Yudistiawan, S. Ansumali, and I. V. Karlin, Hydrodynamics beyond Navier-Stokes: The slip flow model, Phys. Rev. E **78**, 016705 (2008).

[22] W. P. Yudistiawan, S. K. Kwak, D. V. Patil, and S. Ansumali, Higher-order Galilean-invariant lattice Boltzmann model for microflows: Single-component gas, Phys. Rev. E **82**, 046701 (2010).

[23] S. Succi, *The Lattice Boltzmann Equation: For Fluid Dynamics and Beyond* (Oxford University Press, New York, 2001).

[24] Z. Guo, C. Zheng, and B. Shi, Discrete lattice effects on the forcing term in the lattice Boltzmann method, Phys. Rev. E **65**, 046308 (2002).

[25] Y. Zhou, R. Zhang, I. Staroselsky, H. Chen, W. T. Kim, and M. S. Jhon, Simulation of micro-and nano-scale flows via the lattice Boltzmann method, Physica A **362**, 68 (2006).

[26] R. Zhang, X. Shan, and H. Chen, Efficient kinetic method for fluid simulation beyond the Navier-Stokes equation, Phys. Rev. E **74**, 046703 (2006).

[27] J. Latt and B. Chopard, Lattice Boltzmann method with regularized pre-collision distribution functions, Math. Comput. Simulation **72**, 165 (2006).

[28] A. Montessori, P. Prestininzi, M. La Rocca, and S. Succi, Lattice Boltzmann approach for complex nonequilibrium flows, Phys. Rev. E **92**, 043308 (2015).

[29] A. Montessori, G. Falcucci, P. Prestininzi, M. La Rocca, and S. Succi, Regularized lattice Bhatnagar-Gross-Krook model for two-and three-dimensional cavity flow simulations, Phys. Rev. E **89**, 053317 (2014).

[30] F. J. Higuera, S. Succi, and R. Benzi, Lattice gas dynamics with enhanced collisions, Europhys. Lett. **9**, 345 (1989).

[31] A. Montessori, P. Prestininzi, M. La Rocca, G. Falcucci, and S. Succi, Lattice kinetic approach to non-equilibrium flows, in *International Conference of Numerical Analysis and Applied Mathematics 2015*, edited by T. Simos and C. Tsitouras (AIP Melville, NY, 2016), Vol. 1738, pp. 090005.

[32] F. Jiang and T. Tsuji, Changes in pore geometry and relative permeability caused by carbonate precipitation in porous media, Phys. Rev. E **90**, 053306 (2014).

[33] T. Tsuji, F. Jiang, and K. T. Christensen, Characterization of immiscible fluid displacement processes with various capillary numbers and viscosity ratios in 3d natural sandstone, Advances Water Res. **95**, 3 (2016).

[34] A. Beskok and G. E. Karniadakis, Report: A model for flows in channels, pipes, and ducts at micro and nano scales, Microscale Thermophys. Eng. **3**, 43 (1999).

[35] Jianlin Zhao, Jun Yao, Aifen Li, Min Zhang, Lei Zhang, Yongfei Yang, and Hai Sun, Simulation of microscale gas flow in heterogeneous porous media based on the lattice Boltzmann method, J. Appl. Phys. **120**, 084306 (2016).

[36] J. O. Hirschfelder, C. F. Curtiss, R. B. Bird, and M. G. Mayer, *Molecular Theory of Gases and Liquids* (Wiley New York, 1954), Vol. 26.

[37] K. Suga, S. Takenaka, T. Ito, M. Kaneda, T. Kinjo, and S. Hyodo, Evaluation of a lattice Boltzmann method in a complex nanoflow, Phys. Rev. E **82**, 016701 (2010).

[38] X. D. Dong Niu, S. A. Hyodo, T. Munekata, and K. Suga, Kinetic lattice Boltzmann method for microscale gas flows: Issues on boundary condition, relaxation time, and regularization, Phys. Rev. E **76**, 036711 (2007).

[39] Pierre Lallemand and Li-Shi Luo, Theory of the lattice Boltzmann method: Dispersion, dissipation, isotropy, galilean invariance, and stability, Phys. Rev. E **61**, 6546 (2000).

[40] Irina Ginzburg and Dominique d'Humières, Multireflection boundary conditions for lattice boltzmann models, Phys. Rev. E **68**, 066614 (2003).

[41] Siarhei Khirevich, Irina Ginzburg, and Ulrich Tallarek, Coarse-and fine-grid numerical behavior of MRT/TRT lattice-Boltzmann schemes in regular and random sphere packings, J. Comput. Phys. **281**, 708 (2015).

[42] Zhaoli Guo, Jishun Qin, and Chuguang Zheng, Generalized second-order slip boundary condition for nonequilibrium gas flows, Phys. Rev. E **89**, 032120 (2014).